

## Spontaneous flow instabilities of active polar fluids in three dimensions

Abhinav Singh <sup>1,2,3,4,\*</sup>, Quentin Vagne,<sup>5</sup> Frank Jülicher,<sup>6,3,7</sup> and Ivo F. Sbalzarini <sup>1,2,3,7,4,†</sup>

<sup>1</sup>Faculty of Computer Science, Technische Universität Dresden, Dresden, Germany

<sup>2</sup>Max Planck Institute of Molecular Cell Biology and Genetics, Dresden, Germany

<sup>3</sup>Center for Systems Biology Dresden, Dresden, Germany

<sup>4</sup>Center for Scalable Data Analytics and Artificial Intelligence ScaDS.AI, Dresden/Leipzig, Germany

<sup>5</sup>University of Geneva, Geneva, Switzerland

<sup>6</sup>Max Planck Institute for the Physics of Complex Systems, Dresden, Germany

<sup>7</sup>Cluster of Excellence Physics of Life, TU Dresden, Dresden, Germany



(Received 24 January 2023; accepted 9 June 2023; published 22 June 2023)

Active polar fluids exhibit spontaneous flow when sufficient active stress is generated by internal molecular mechanisms. This is also referred to as an active Fréedericksz transition. Experiments have revealed the existence of competing in-plane and out-of-plane instabilities in three-dimensional active matter. So far, however, a theoretical model reconciling all observations is missing. In particular, the role of boundary conditions in these instabilities still needs to be explained. Here, we characterize the spontaneous flow transition in a symmetry-preserving three-dimensional active Ericksen-Leslie model, showing that the boundary conditions select the emergent behavior. Using nonlinear numerical solutions and linear perturbation analysis, we explain the mechanism for both in-plane and out-of-plane instabilities under extensile active stress for perpendicular polarity anchoring at the boundary, whereas parallel anchoring only permits in-plane flows under contractile stress or out-of-plane wrinkling under extensile stress.

DOI: [10.1103/PhysRevResearch.5.L022061](https://doi.org/10.1103/PhysRevResearch.5.L022061)

**Introduction.** Active fluids are out-of-equilibrium materials driven by energy injection at the microscopic scale [1,2]. Active materials can have a polar or nematic alignment symmetry of the orientation vector field, and the constituents of the material allow it to generate contractile or extensile active stress. Prominent examples of active fluids are found in living matter across scales, from the cytoskeleton [3,4] and tissues [5–7] to collective behavior in flocks [8]. The hydrodynamic theory of incompressible active polar fluids describes the dynamics of such active liquid crystals at long wavelengths. A key behavior of active polar fluids is their ability to generate spontaneous flow under confinement and sufficient active stress. It has been shown in two dimensions (2D) that spontaneous flow can emerge due to a Fréedericksz-type transition first observed in passive liquid crystals [9]. The passive Fréedericksz transition describes the change of a homogeneous nematic state to an inhomogeneous state under the influence of external electric or magnetic fields [10]. In active liquid crystals, the transition is driven by active molecular processes causing spontaneous material flow [11–16].

In two dimensions, the type of instability depends on the confining boundary condition for the polarity field [4], as illustrated in Fig. 1. For polarity anchored perpendicular to boundaries, one obtains a spontaneous flow transition with extensile active stress [Figs. 1(a) and 1(b)] [12]. For polarity parallel to the boundary, the transition occurs for contractile active stress [Figs. 1(c) and 1(d)] [13,16].

Recent works suggest such instabilities to also exist in three-dimensional (3D) active polar fluids [17–20]. For example, an extensile active fluid was found to exhibit a bending instability in a minimal model [21], and flow-aligning active fluids were found to display coherent motion in 3D channels upon increased activity [22]. Furthermore, it has been shown that 3D contractile active fluids dampen out-of-plane perturbations, whereas extensile fluids amplify them in the absence of boundary effects [23]. 3D active fluids under confinement behave fundamentally different from their 2D counterparts. Notably, they exhibit flow due to buckling under extensile active stress, which is not possible in 2D for rigid boundaries [17]. Experimentally, such instabilities have been observed in microtubule assays capable of generating extensile active stresses [17,18]. Some experiments suggested that in-plane and out-of-plane instabilities compete, depending on the material properties and the magnitude of the active stress [19,20]. Other experiments [18] found only an out-of-plane instability. Currently, a theoretical model explaining and reconciling all observations is missing, and the dependence of the instability on the relevant system parameters and boundary conditions remains unexplained.

Here, we study the symmetry-preserving active Ericksen-Leslie hydrodynamic model with a Lagrange multiplier

\*absingh@mpi-cbg.de

†ivos@mpi-cbg.de

Published by the American Physical Society under the terms of the [Creative Commons Attribution 4.0 International license](https://creativecommons.org/licenses/by/4.0/). Further distribution of this work must maintain attribution to the author(s) and the published article's title, journal citation, and DOI. Open access publication funded by the Max Planck Society.

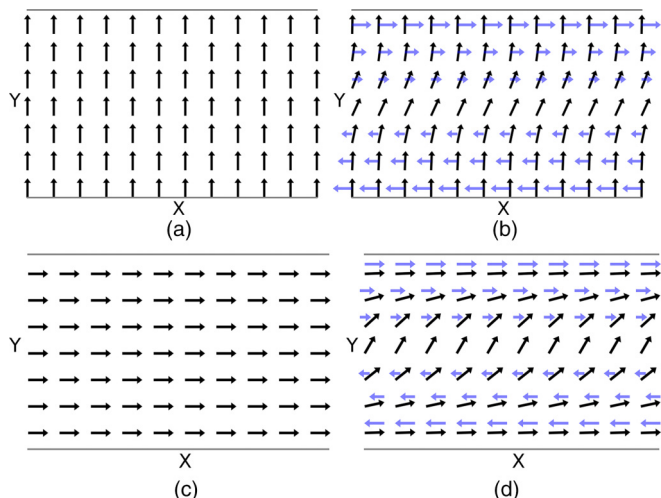


FIG. 1. Two-dimensional active spontaneous flow transition in a plane that is infinite along  $X$  and of finite width  $L$  along  $Y$ . (a) An initially homogeneous polarity field with perpendicular anchoring to the walls and no flow. (b) Spontaneous flow transition under *extensile* active stress with velocity indicated by blue arrows. (c) An initially homogeneous polarity field with parallel anchoring at the walls and no flow. (d) Transition to spontaneous flow under *contractile* active stress.

enforcing constant polarity magnitude. This allows us to show that the effect of orientational order is sufficient to account for all observed instabilities in 3D. We consider a thick active polar film, which is the 3D extension of a *Fréedericksz cell*, with anchoring of the polarity and stress-free boundary conditions on the walls. We explain how steady-state spontaneous flows can arise for different system sizes, polarity boundary conditions, and active stress signs/magnitudes. We derive analytical expressions for the critical activity or length scale by linear perturbation analysis, analogous to the seminal work of Voituriez *et al.* in 2D [16]. We confirm the analytical results in convergence-validated direct 3D numerical solutions of the

full nonlinear model with Lagrange multipliers and complex boundary conditions.

We find a transition in 3D for perpendicular anchoring under extensile active stress (Fig. 2). This transition is different from the 2D case [Fig. 1(a)] as the resulting shear flow is both along the  $X$  and  $Z$  directions [Fig. 2(c)]. This leads to out-of-plane bending of the polarity and to a 3D spontaneous flow transition that is invariantly extended along the  $X$  and  $Z$  directions [Fig. 2(b)]. For parallel anchoring at the wall, we find a transition with contractile active stress that impedes out-of-plane perturbations and is an invariant extension of the 2D spontaneous flow transition [Figs. 3(b) and 3(c)], and a purely out-of-plane “wrinkling” under extensile active stress that does not exist in 2D [Figs. 3(d)–3(f)].

*Hydrodynamics of active polar fluids.* The incompressible viscous active polar fluid equations [1] can be described in Einstein summation notation as

$$\frac{Dp_\alpha}{Dt} = \frac{h_\alpha}{\gamma} - \nu u_{\alpha\beta} p_\beta + \lambda \Delta \mu p_\alpha, \quad (1a)$$

$$\partial_\beta \sigma_{\alpha\beta}^{(\text{tot})} - \partial_\alpha \Pi = 0, \quad \partial_\gamma v_\gamma = 0, \quad (1b)$$

$$2\eta u_{\alpha\beta} = \sigma_{\alpha\beta}^{(s)} + \zeta \Delta \mu \left( p_\alpha p_\beta - \frac{1}{3} p_\gamma p_\gamma \delta_{\alpha\beta} \right) - \frac{\nu}{2} \left( p_\alpha h_\beta + p_\beta h_\alpha - \frac{2}{3} p_\gamma h_\gamma \delta_{\alpha\beta} \right), \quad (1c)$$

with  $\alpha, \beta, \gamma \in \{x, y, z\}$  for the spatial components. Further details can be found in the Supplemental Material [24]. This model fulfills the Onsager symmetry relations and accounts for stresses from elastic distortion of the nematic field, as well as antisymmetric and Ericksen stresses. The scalar  $\nu$  is the standard liquid-crystal flow aligning/tumbling parameter. The molecular field  $\mathbf{h} = K \nabla^2 \mathbf{p} + h_{\parallel}^0 \mathbf{p}$  can be decomposed into parallel  $h_{\parallel} = \mathbf{p} \cdot \mathbf{h}$  and perpendicular  $\mathbf{h}_{\perp} = \mathbf{p} \times \mathbf{h}$  components in a local comoving frame. Note that molecular fields differing by a factor of  $h_{\parallel}^0 \mathbf{p}$  are equivalent [25] and hence  $h_{\parallel} = h_{\parallel}^0$ . Using Eq. (1a) and enforcing  $p_\gamma \frac{Dp_\gamma}{Dt} = 0$ ,  $h_{\parallel}$  can be

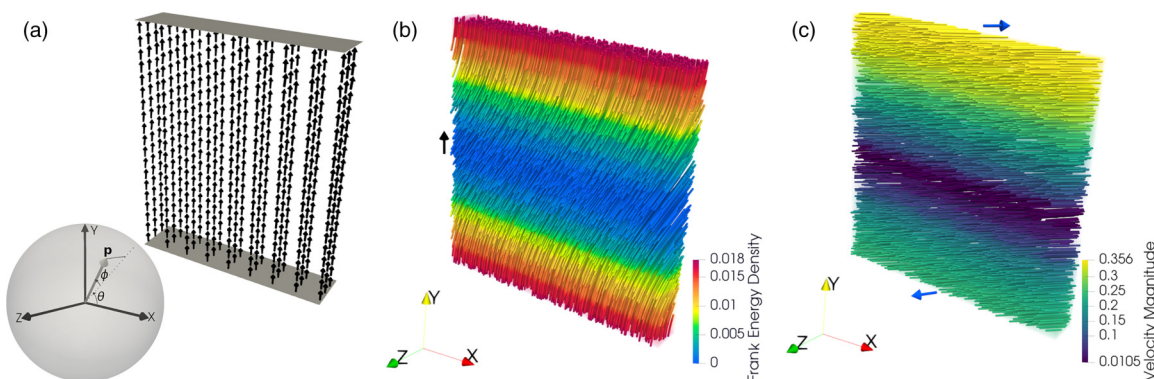


FIG. 2. Visualization of the 3D spontaneous flow transition for perpendicular polarity anchoring at the wall under extensile active stress. (a) Coordinate system and the homogeneous steady state: Polarity vectors below the critical active potential ( $\Delta \tilde{\mu} < \Delta \tilde{\mu}_c$ ). (b) Polarity field in the spontaneous flow steady state: Polarity streamlines with nonzero polarity in both  $X$  and  $Z$  directions, and Frank free-energy density as color. The black arrow indicates the initial polarity vector direction. (c) Velocity field in the spontaneous flow steady state: Velocity streamlines for the spontaneous flow steady state in (b) with nonzero flow in both  $X$  and  $Z$  directions, with velocity magnitude as color. The blue arrows indicate the directions of the flow at the stress-free walls.

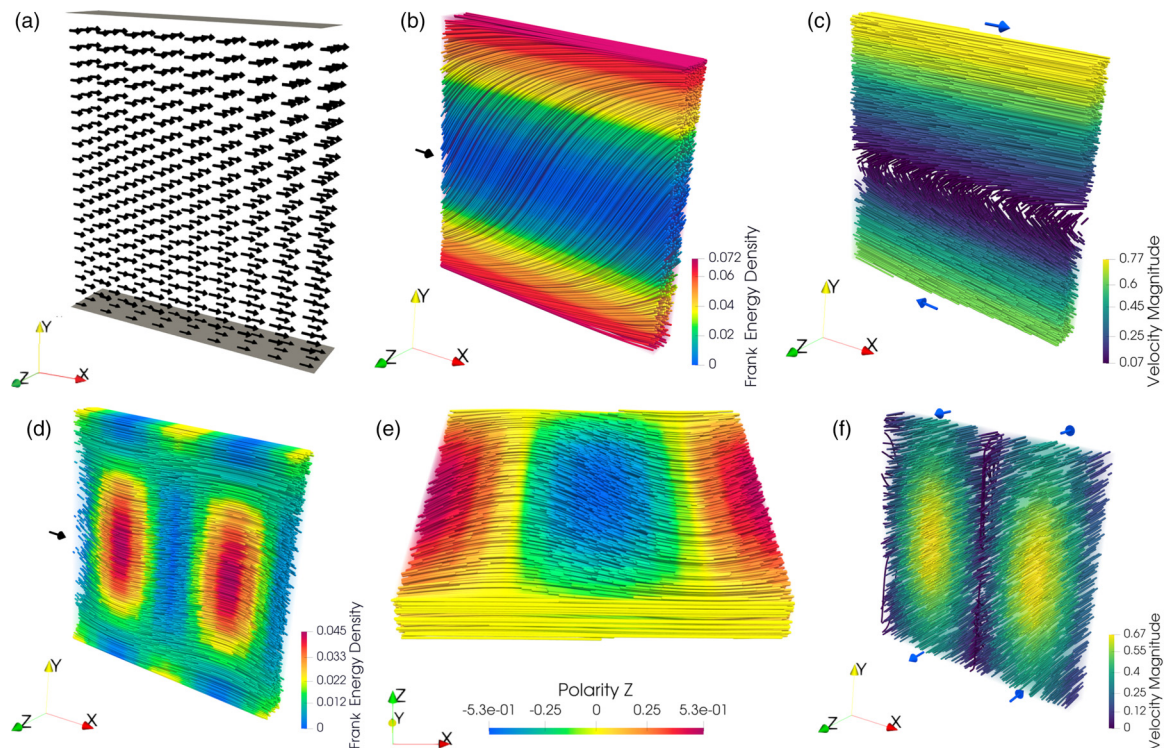


FIG. 3. Visualization of the 3D spontaneous flow transitions with parallel polarity anchoring at the wall. (a) Homogeneous steady state: Polarity vectors below the critical active potential ( $\Delta\tilde{\mu} < \Delta\tilde{\mu}_c$ ). (b) In-plane spontaneous flow steady state under contractile active stress: Polarity streamlines showing nonzero polarity in the  $Y$  direction and zero in the  $Z$  direction, with Frank free-energy density as color. The black arrow indicates the initial polarity vector direction. (c) Velocity field in the spontaneous flow steady state under contractile active stress: Velocity streamlines for the in-plane spontaneous flow steady state in (b) with nonzero flow in the  $X$  direction and velocity magnitude as color. The blue arrows indicate the directions of the flow at the stress-free walls. Parameter values for (b) and (c) are  $\tilde{\gamma} = 1$ ,  $\tilde{L} = 10$ ,  $\tilde{\nu} = -0.4$ ,  $\tilde{\zeta} = -1$ ,  $\Delta\tilde{\mu} = 0.35$ . (d) Out-of-plane spontaneous flow steady state under extensile active stress: Polarity streamlines showing nonzero polarity field in the  $Z$  direction and zero in the  $Y$  direction, with Frank free-energy density as color. The black arrow indicates the initial polarity vector direction. (e)  $Z$  component of the polarity field in the out-of-plane spontaneous flow steady state under extensile active stress. (f) Velocity in the out-of-plane spontaneous flow steady state under extensile active stress: Velocity streamlines for the spontaneous flow steady state under extensile active stress in (d) with nonzero flow in the  $Z$  direction and velocity magnitude as color. The blue arrows indicate the directions of the flow at the stress-free walls. Parameter values for (d)–(f) are  $\tilde{\gamma} = 1$ ,  $\tilde{L} = 10$ ,  $\tilde{\nu} = -0.4$ ,  $\tilde{\zeta} = 1$ ,  $\Delta\tilde{\mu} = 2.4$ .

derived as  $h_{\parallel} = -\gamma[\lambda\Delta\mu - \frac{2\nu}{P_{\gamma}P_{\gamma}}(u_{\alpha\beta}P_{\alpha}P_{\beta})]$ , such that  $\|\mathbf{p}\|$  remains constant. In 2D, the perpendicular component of the molecular field is a scalar with one degree of freedom, which makes the nonlinear equations analytically tractable. In 3D, however,  $\mathbf{h}_{\perp} = (h_{\perp x}, h_{\perp y}, h_{\perp z})$  is a 3-vector, and the coupling of the Frank free energy with the Lagrange multiplier  $h_{\parallel}$  renders the force-balance equation intricate. Therefore, it is not clear from simplified models how the flow instability depends on system parameters such as  $\lambda$ ,  $\zeta$ , or  $\nu$  [17,21]. The microscopic origin of  $\lambda$  and  $\zeta$ , however, can be elucidated in the full nonlinear model, providing experimentally measurable predictions.

**Results.** We analyze the hydrodynamic equations (1) at steady state and provide a mechanism for the emergence of symmetry-breaking spontaneous flow. We express the unit polarity vector as  $\mathbf{p} = [\cos(\theta)\cos(\phi), \sin(\theta)\cos(\phi), \sin(\phi)]$  using the coordinates illustrated in Fig. 2. We eliminate the velocity from Eq. (1) and obtain the nonlinear force balance equation as a function of  $(\theta, \phi)$ . For anchoring boundary conditions  $(\theta_0, \phi_0)$  at the top and bottom walls, the system is steady with trivial solution  $[\theta(y), \phi(y)] = (\theta_0, \phi_0)$ .

For the case of perpendicular anchoring of the polarity at the boundary, i.e.,  $(\theta_0, \phi_0) = (\frac{\pi}{2}, 0)$ , assuming small perturbations  $[\epsilon(y), \kappa(y)]$  around the no-flow homogeneous steady state, we obtain the equations for the perturbations by linearizing the nonlinear equation

$$K \frac{\partial^2}{\partial y^2} \begin{bmatrix} \epsilon(y) \\ \kappa(y) \end{bmatrix} = \frac{2\gamma\Delta\mu(\nu-1)(\zeta + \gamma\lambda\nu)}{\gamma(\nu-1)^2 + 4\eta} \begin{bmatrix} \epsilon(y) \\ \kappa(y) \end{bmatrix}. \quad (2)$$

Hence, there are perturbation modes of the form

$$\begin{bmatrix} \epsilon(y) \\ \kappa(y) \end{bmatrix} = \sin\left(\frac{\pi}{L}y\right) \begin{bmatrix} \epsilon_m \\ \kappa_m \end{bmatrix}, \quad (3)$$

where  $\epsilon_m, \kappa_m$  are the maximum tilt magnitudes in  $\theta$  and  $\phi$ , respectively. These modes effectively define a critical activity

$$\Delta\mu_c = \frac{K\pi^2[4\eta + \gamma(\nu-1)^2]}{2L^2\gamma(\nu-1)(-\zeta - \gamma\lambda\nu)}. \quad (4)$$

Assuming  $-1 < \nu < 1$ , and for perpendicular anchoring of polarity, we note that for the critical  $\Delta\mu_c > 0$  the effective active stress is extensile,  $-\zeta - \gamma\lambda\nu < 0$ . Hence for a flow-tumbling polarity, we expect the spontaneous flow transition

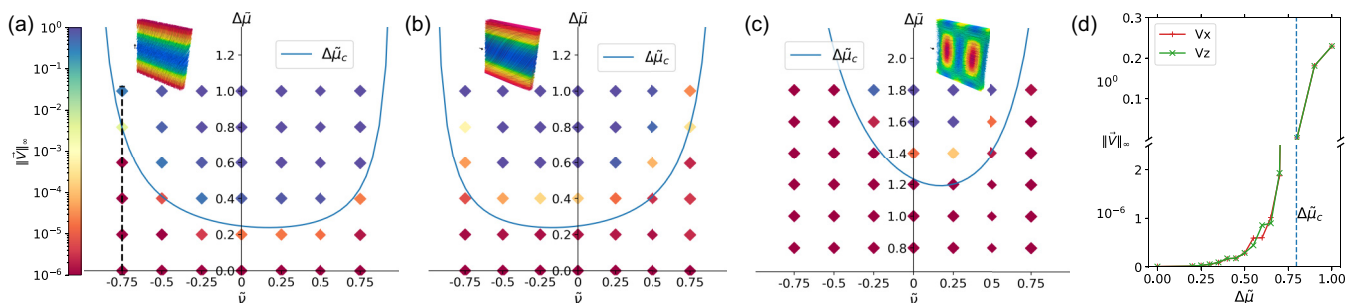


FIG. 4. Transition for different flow regimes. The solid lines plot the analytical expressions for the dimensionless critical activity  $\Delta\tilde{\mu}_c$  vs dimensionless flow-tumbling parameter  $\tilde{\nu}$  for  $\tilde{\gamma} = \tilde{\zeta} = 1$  and  $\tilde{L} = 10$ . The color of the  $\blacklozenge$  symbols in the background grid indicates the maximum norm of the spontaneous flow velocity obtained by numerically solving the nonlinear equations at those parameters with a tolerance of  $10^{-6}$ . (a) Perpendicular polarity anchoring with extensile stress, Eq. (4). See (d) for more simulations along the dashed line. (b) Parallel anchoring with contractile stress, Eq. (7). (c) Parallel anchoring with extensile stress, Eq. (10). (d) Numerically obtained maximum flow velocity magnitude vs activity  $\Delta\tilde{\mu}$  for  $\tilde{\nu} = -0.75$  [dashed vertical line in (a)] for spontaneous flow with perpendicular anchoring and extensile active stress. Note the broken Y axis with different scales to accommodate for the sharp increase around the critical activity  $\Delta\tilde{\mu}_c$ .

when  $\Delta\mu > \Delta\mu_c$ . However, the instability depends on a nonlinear combination of parameters. For example, the critical activity depends nonlinearly on  $\nu$ . Further, the effects of  $\zeta$  and  $\lambda$  are coupled to both the rotational viscosity  $\gamma$  and to  $\nu$ . For  $|\nu| > 1$ , the behavior depends on  $|\zeta|$ . We provide phase diagrams for these three qualitatively different critical behaviors in Supplemental Material SM3 [24].

The governing equations can be nondimensionalized with respect to  $\lambda$ ,  $\eta$ , and  $K$  by rescaling  $\tilde{L} = (\eta\lambda)^{\frac{1}{3}}L$ ,  $\tilde{\zeta} = \zeta(\eta\lambda)^{-1}$ ,  $\Delta\tilde{\mu} = \Delta\mu(\eta\lambda)^{\frac{1}{3}}K^{-1}$ ,  $\tilde{\gamma} = \gamma\eta^{-1}$ , and  $\tilde{\nu} = \nu$ . We numerically solve the dimensionless equations for a thick 3D active film that is periodic along the  $X$  and the  $Z$  directions and has thickness  $L$  in the  $Y$  direction. Details of the simulation method can be found in SM2 [24]. The simulation computer code scales to parallel computer architectures, as it is based on the open-source scientific computing library OpenFPM [26] and a template expression language for partial differential equations [27].

We verify the expressions in Eq. (4) by numerically solving the nonlinear equations for  $\tilde{\gamma} = 1$ ,  $\tilde{\zeta} = 1$ ,  $\tilde{L} = 10$ . For these parameters, the dependence of the critical activity ( $\Delta\tilde{\mu}_c$ ) on the flow-tumbling parameter  $\tilde{\nu}$  is shown in Fig. 4(a) as a solid line. Hence, when  $\Delta\tilde{\mu} > \Delta\tilde{\mu}_c$ , the mode in Eq. (3) appears with spontaneous flow governed by

$$\frac{\partial}{\partial y} \begin{bmatrix} v_x(y) \\ v_z(y) \end{bmatrix} = \frac{2\Delta\mu(\gamma\lambda\nu + \zeta)}{\gamma(\nu - 1)^2 + 4\eta} \begin{bmatrix} -\epsilon(y) \\ \kappa(y) \end{bmatrix}. \quad (5)$$

We find that the mode may be stabilized by the nonlinearities above the critical potentials, resulting in steady-state flows. In the steady flow state, active stresses are balanced by elastic nematic stresses, leading to stationary perturbation modes. The corresponding spontaneous flow transition is observed above the critical activity and is visualized in Fig. 2 and SM Video I [24].

We study the stability of parallel anchoring of the polarity at the boundary, i.e.,  $(\theta_0, \phi_0) = (0, 0)$ . We again linearize around small angle perturbations  $(\epsilon, \kappa)$  of the polarity and

obtain

$$K \frac{\partial^2}{\partial y^2} \begin{bmatrix} \epsilon(y) \\ \kappa(y) \end{bmatrix} = \frac{2\gamma\Delta\mu(\nu + 1)(\gamma\lambda\nu + \zeta)}{\gamma(\nu + 1)^2 + 4\eta} \begin{bmatrix} \epsilon(y) \\ 0 \end{bmatrix}. \quad (6)$$

This leads to a critical activity

$$\Delta\mu_c = \frac{\pi^2 K [4\eta + \gamma(\nu + 1)^2]}{2\gamma L^2 (\nu + 1)(-\zeta - \gamma\lambda\nu)}. \quad (7)$$

For the critical  $\Delta\mu_c > 0$ , and parallel anchoring of the polarity field, the active stress for the transition is contractile,  $-\zeta - \gamma\lambda\nu > 0$ , giving rise to a spontaneous flow transition with an  $S$ -like shape of the polarity field [Fig. 3(b)], as observed in 2D, but invariantly extended in the third dimension. This confirms that contractile active polar fluids impede out-of-plane perturbations when polarity is anchored on the boundary. The spontaneous flow transition occurs when  $\Delta\mu > \Delta\mu_c$ . We confirm this in nonlinear simulations for the same parameters as before and  $\tilde{\zeta} = -1$ . The dependence of the critical activity for contractile active stress on the flow-tumbling parameter  $\tilde{\nu}$  is plotted in Fig. 4(b) as a solid line. The numerical solutions for  $\Delta\tilde{\mu} > \Delta\tilde{\mu}_c$  confirm the transition for different values of  $\nu$ , and the maximum norm of the flow velocity is shown as a color code in Fig. 4(b). The initial homogeneous state of polarity is shown in Fig. 3(a). Figure 3(b) shows the polarity field for the steady-state spontaneous flow shown in Fig. 3(c). The onset of this transition is also shown in SM Video II [24].

We note that the symmetry can also be broken in the  $X$  direction instead of  $Y$ , such that  $u_{xz} \neq 0$  and  $u_{xy} = 0$ . A similar analysis then reveals a 2D extensile perturbation mode,

$$K \nabla_{[x,y]}^2 \begin{bmatrix} \epsilon(x, y) \\ \kappa(x, y) \end{bmatrix} = \frac{-2\gamma\Delta\mu(\nu - 1)(\gamma\lambda\nu + \zeta)}{\gamma(\nu - 1)^2 + 4\eta} \begin{bmatrix} 0 \\ \kappa(x, y) \end{bmatrix}. \quad (8)$$

This leads to perturbations of the form

$$\kappa(x, y) = \kappa_m \cos\left(\frac{2\pi}{L_x}x + \alpha\right) \sin\left(\frac{\pi}{L_y}y\right), \quad (9)$$

where  $\alpha$  is the phase shift, which is fixed by the flow boundary condition and the integration constant. This mode corresponds

to a critical activity

$$\Delta\mu_c = \frac{(4L_x^2 + L_y^2)\pi^2 K[\gamma(\nu - 1)^2 + 4\eta]}{2\gamma L_x^2 L_y^2 (\nu - 1)(-\zeta - \gamma\lambda\nu)}. \quad (10)$$

For the critical  $\Delta\mu_c > 0$ , and parallel anchoring, the active stress for the transition is extensile,  $-\zeta - \gamma\lambda\nu < 0$ . The mode in Eq. (9) describes an out-of-plane transition maintaining  $\theta(x, y) = 0$ . For the previously chosen parameters and  $\zeta = 1$ , the dependence of  $\Delta\tilde{\mu}_c$  on  $\tilde{\nu}$  is shown in Fig. 4(c).

The above expressions further clarify the effect of the finite length  $L_x$  of the domain in the  $X$  direction. In the ideal physical system,  $L_x$  is infinite, and  $L_y$  is finite. In Eq. (10), we see that there is a nonzero limit for the critical activity as  $L_x$  approaches infinity, and the mode of deformation in Eq. (9) has no modulation in the  $X$  direction. This predicts the wrinkling wavelength close to the transition. For further increasing activity, however, the perturbations are no longer small, rendering the linearized equations invalid. Then, the system transitions to spatiotemporal chaos.

The amplitudes  $\epsilon_m, \kappa_m$  depend on  $\Delta\tilde{\mu}$  and are analytically intractable. The critical active potential for out-of-plane wrinkling is significantly larger than for the other cases. This causes the instability to occur earlier or faster in time in 3D. The unstable mode shows oscillatory flows in opposite directions. With  $\Delta\tilde{\mu} > \Delta\tilde{\mu}_c$ , we find a spontaneous flow transition of small amplitude near the critical value, as shown by the maximum norm of the velocity (color of symbols). The associated wrinkling in the transition is shown in Figs. 3(d)–3(f) and SM Video III [24]. This transition has also been observed experimentally in extensile polar fluids and referred to as *bending* or *wrinkling instability* [17–20]. Here, we qualitatively characterized the effect of finite channel length  $L_x$  on the wrinkling wavelength.

**Conclusions.** We have derived the critical active stress for the spontaneous flow transition in 3D active liquid crystals from the full, symmetry-preserving active Ericksen-Leslie model with Lagrange multipliers. We found that contractile active stresses impede out-of-plane perturbations at the transition, whereas extensile active stresses promote them under parallel anchoring of the polarity at the walls. For perpendicular polarity boundary conditions, we found a 3D active Fréedericksz-type transition under purely extensile stress. We

analytically derived the critical active potentials for the transition in each case and confirmed them in direct numerical solutions of the nonlinear 3D system. For a fixed activity  $\Delta\mu$ , the present analysis equivalently yields a corresponding critical length  $L_c$  that defines a system size above which the transition occurs. The results show how the instabilities arise from the interplay between the boundary conditions, the active potential, and the channel width and length.

Our work can be related to previous studies on similar systems. Similar in-plane and out-of-plane instabilities as described here were previously reported using hybrid lattice-Boltzmann simulations with periodic boundary conditions [23]. However, for flow-tumbling active fluids, another study reported no coherent flow in 3D channels without preferential anchoring on the boundaries [22]. Here, we have shown that such flows do occur if the polarity field is anchored at the surfaces. Interestingly, a simplified model generated pumping behavior without anchoring boundary conditions when no-slip velocity boundary conditions were used [21]. We verified that for the no-slip boundary conditions, such behavior also occurs in our model for supercritical activity. We then observe the same flow modes as previously seen in 2D [16].

Our results accurately predict the type of spontaneous flow in 3D and provide a comprehensive understanding of 3D active fluids, unifying previously made observations and explaining their physical origin. We have shown how 3D active matter differs from its 2D counterpart due to the additional degrees of freedom. Indeed, we found a bending or wrinkling instability mediating spontaneous flow in 3D, explaining earlier experimental observations [17–20] with direct implications for understanding biological morphogenesis and finding design principles for the control of active matter.

**Acknowledgments.** This work was supported by the Center for Scalable Data Analytics and Artificial Intelligence (ScaDS.AI) Dresden/Leipzig, funded by the Federal Ministry of Education and Research (BMBF, Bundesministerium für Bildung und Forschung). We thank the Scientific Computing Facility of MPI-CBG and the Center for Information Services and High Performance Computing (ZIH) of TU Dresden for providing the compute resources for the numerical simulations. We thank Philipp Suhrcke (Sbalzarini group) and the anonymous referees for their constructive comments.

- 
- [1] F. Jülicher, S. W. Grill, and G. Salbreux, Hydrodynamic theory of active matter, *Rep. Prog. Phys.* **81**, 076601 (2018).
  - [2] M. J. Bowick, N. Fakhri, M. C. Marchetti, and S. Ramaswamy, Symmetry, Thermodynamics, and Topology in Active Matter, *Phys. Rev. X* **12**, 010501 (2022).
  - [3] K. Kruse, J.-F. Joanny, F. Jülicher, J. Prost, and K. Sekimoto, Generic theory of active polar gels: A paradigm for cytoskeletal dynamics, *Eur. Phys. J. E* **16**, 5 (2005).
  - [4] F. Jülicher, K. Kruse, J. Prost, and J. F. Joanny, Active behavior of the cytoskeleton, *Phys. Rep.* **449**, 3 (2007).
  - [5] A. C. Martin, Pulsation and stabilization: Contractile forces that underlie morphogenesis, *Dev. Biol.* **341**, 114 (2010).
  - [6] S. Shankar, A. Souslov, M. J. Bowick, M. C. Marchetti, and V. Vitelli, Topological active matter, *Nat. Rev. Phys.* **4**, 380 (2022).
  - [7] P. Guillamat, C. Blanch-Mercader, G. Pernellet, K. Kruse, and A. Roux, Integer topological defects organize stresses driving tissue morphogenesis, *Nat. Mater.* **21**, 588 (2022).
  - [8] M. C. Marchetti, J. F. Joanny, S. Ramaswamy, T. B. Liverpool, J. Prost, M. Rao, and R. A. Simha, Hydrodynamics of soft active matter, *Rev. Mod. Phys.* **85**, 1143 (2013).
  - [9] V. Fréedericksz and V. Zolina, Forces causing the orientation of an anisotropic liquid, *Trans. Faraday Soc.* **29**, 919 (1933).

- [10] S. Shoarinejad and M. Shahzamanian, On the numerical study of Frederick transition in nematic liquid crystals, *J. Mol. Liq.* **138**, 14 (2008).
- [11] G. Duclos, C. Blanch-Mercader, V. Yashunsky, G. Salbreux, J.-F. Joanny, J. Prost, and P. Silberzan, Spontaneous shear flow in confined cellular nematics, *Nat. Phys.* **14**, 728 (2018).
- [12] R. Ramaswamy, G. Bourantas, F. Jülicher, and I. F. Sbalzarini, A hybrid particle-mesh method for incompressible active polar viscous gels, *J. Comput. Phys.* **291**, 334 (2015).
- [13] S. Ramaswamy, Active fluids, *Nat. Rev. Phys.* **1**, 640 (2019).
- [14] F. G. Woodhouse and R. E. Goldstein, Spontaneous Circulation of Confined Active Suspensions, *Phys. Rev. Lett.* **109**, 168105 (2012).
- [15] H. Wioland, F. G. Woodhouse, J. Dunkel, J. O. Kessler, and R. E. Goldstein, Confinement Stabilizes a Bacterial Suspension into a Spiral Vortex, *Phys. Rev. Lett.* **110**, 268102 (2013).
- [16] R. Voituriez, J. F. Joanny, and J. Prost, Spontaneous flow transition in active polar gels, *Europhys. Lett.* **70**, 404 (2005).
- [17] P. Chandrakar, M. Varghese, S. A. Aghvami, A. Baskaran, Z. Dogic, and G. Duclos, Confinement Controls the Bend Instability of Three-Dimensional Active Liquid Crystals, *Phys. Rev. Lett.* **125**, 257801 (2020).
- [18] T. Strübing, A. Khosravanizadeh, A. Vilfan, E. Bodenschatz, R. Golestanian, and I. Guido, Wrinkling instability in 3D active nematics, *Nano Lett.* **20**, 6281 (2020).
- [19] B. Najma, M. Varghese, L. Tsidilkovski, L. Lemma, A. Baskaran, and G. Duclos, Competing instabilities reveal how to rationally design and control active crosslinked gels, *Nat. Commun.* **13**, 6465 (2022).
- [20] G. Sarfati, A. Maitra, R. Voituriez, J.-C. Galas, and A. Estevez-Torres, Crosslinking and depletion determine spatial instabilities in cytoskeletal active matter, *Soft Matter* **18**, 3793 (2022).
- [21] M. Varghese, A. Baskaran, M. F. Hagan, and A. Baskaran, Confinement-Induced Self-Pumping in 3D Active Fluids, *Phys. Rev. Lett.* **125**, 268003 (2020).
- [22] S. Chandragiri, A. Doostmohammadi, J. M. Yeomans, and S. P. Thampi, Flow States and Transitions of an Active Nematic in a Three-Dimensional Channel, *Phys. Rev. Lett.* **125**, 148002 (2020).
- [23] M. R. Nejad and J. M. Yeomans, Active Extensile Stress Promotes 3D Director Orientations and Flows, *Phys. Rev. Lett.* **128**, 048001 (2022).
- [24] See Supplemental Material at <http://link.aps.org/supplemental/10.1103/PhysRevResearch.5.L022061> for model details, simulation methodology, and different critical behaviors.
- [25] P. G. de Gennes and J. Prost, *The Physics of Liquid Crystals*, 2nd ed., International Series of Monographs on Physics (Clarendon Press, Oxford, 1995).
- [26] P. Incardona, A. Leo, Y. Zaluzhnyi, R. Ramaswamy, and I. F. Sbalzarini, OpenFPM: A scalable open framework for particle and particle-mesh codes on parallel computers, *Comput. Phys. Commun.* **241**, 155 (2019).
- [27] A. Singh, P. Incardona, and I. F. Sbalzarini, A C++ expression system for partial differential equations enables generic simulations of biological hydrodynamics, *Eur. Phys. J. E* **44**, 117 (2021).